

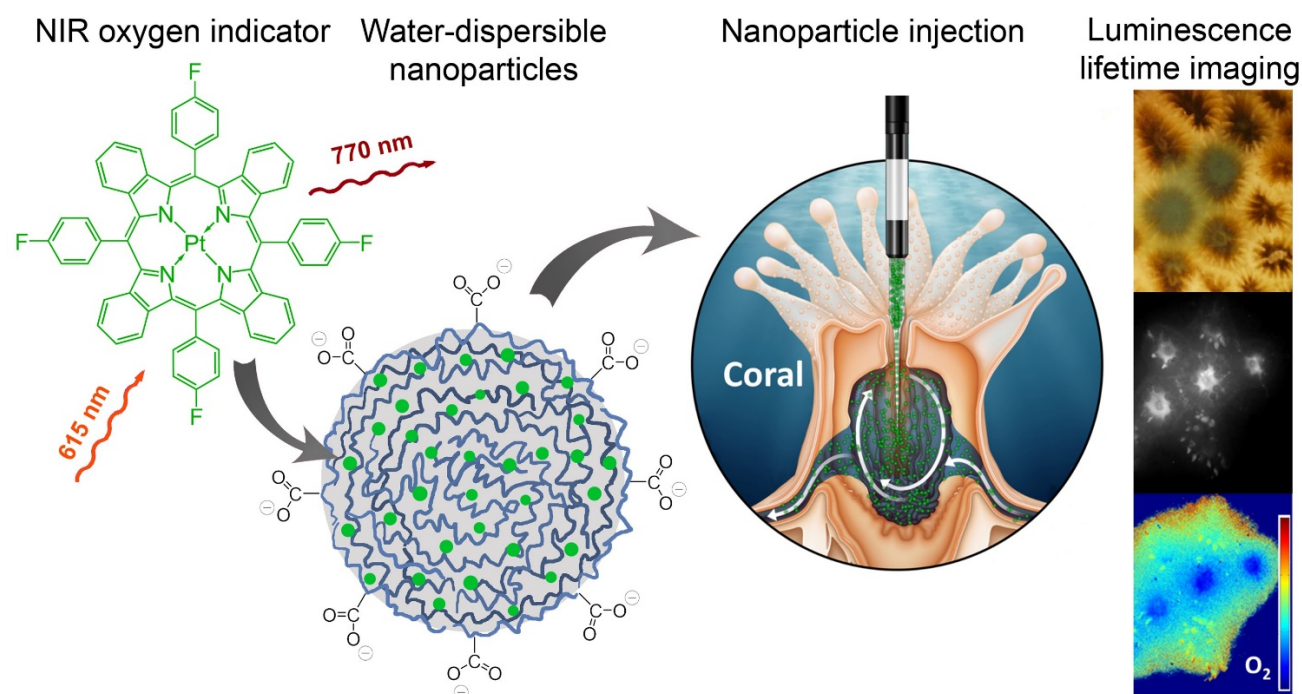
In-vivo Lifetime Imaging of the Internal O₂ Dynamics in Corals with NIR-emitting Sensor Nanoparticles

Michael Kühl^{*,a,b}, Daniel Aagren Nielsen^b and Sergey M. Borisov^{*,c}

^aMarine Biological Section, Department of Biology, University of Copenhagen, Strandpromenaden 5, 3000, Helsingør, Denmark. ^bClimate Change Cluster, University of Technology Sydney, Broadway, 2007, Australia. ^cInstitute of Analytical Chemistry and Food Chemistry, Graz University of Technology, Stremayrgasse 9, A-8010, Graz, Austria

KEYWORDS: *optode, imaging, symbiosis, animal, photosynthesis, respiration.*

ABSTRACT: Mapping of O₂ with luminescent sensors within intact animals is challenging due to attenuation of excitation and emission light caused by tissue absorption and scattering, as well as interfering background fluorescence. Here we show the application of luminescent O₂ sensor nanoparticles (~40-50 nm) composed of the O₂ indicator platinum(II) tetra(4-fluoro)phenyltetrabenzoporphyrin (PtTPTBPF) immobilized in poly(methyl methacrylate-co-methacrylic acid) (PMMA-MA). We injected the sensor nanoparticles into the gastrovascular system of intact colony fractions of reef-building, tropical corals that harbor photosynthetic microalgae in their tissues. The sensor nanoparticles are excited by red LED light (617 nm) and emit in the near-infrared (780 nm), which enhances transmission of excitation and emission light through biological materials. This enabled us to map the internal O₂ concentration via time-domain luminescence lifetime imaging through the outer tissue layers across several coral polyps in flowing seawater. After injection, nanoparticles dispersed within the coral tissue over several hours. While luminescence intensity imaging showed some local aggregation of sensor particles, lifetime imaging showed a more homogenous O₂ distribution across a larger area of the coral colony. Local stimulation of symbiont photosynthesis in corals induced oxygenation of illuminated tissue areas and formation of lateral O₂ gradients toward surrounding respiring tissues, which were dissipated rapidly after onset of darkness. Such measurements are key to improve our understanding of how corals regulate their internal chemical microenvironment and metabolic activity and how they are affected by environmental stress such as ocean warming, acidification and deoxygenation. Our experimental approach can also be adapted for *in vivo* O₂ imaging in other natural systems such as biofilms, plant and animal tissues, as well as in organoids and other cell constructs, where imaging internal O₂ conditions are relevant and challenging due to high optical density and background fluorescence.



INTRODUCTION

Measuring O₂ concentration is a key component in many environmental, physiological or ecological studies, as it is i) consumed in aerobic respiration, ii) produced in oxygenic photosynthesis, and iii) used for reoxidation of reduced products from anaerobic processes. It thus plays an essential role for important physiological and biogeochemical processes in the biosphere (1,2). The solubility of O₂ in water is relatively low, i.e., 1 liter of air contains ca. 30 times more O₂ than a liter of air-saturated water. At the same time, the O₂ transport by diffusion is about 10000 times slower in water than in air. Consequently, aquatic habitats and organisms can undergo strong shifts in their O₂ regime ranging from super-saturated (hyperoxic) conditions over normal air saturated conditions (normoxia) to critical low concentrations (hypoxia) or even anoxia depending on the balance between O₂ formation (via photosynthesis), consumption (via respiration) and transport via diffusion and advection. Excess loading of organic carbon in coastal waters can e.g. lead to strong O₂ depletion via microbial biomass breakdown, causing mortality of marine animals and formation of benthic or planktonic “death” zones, where O₂ is deprived. Currently, climate change is driving an ongoing ocean deoxygenation (3), which already has led to increasing prevalence of hypoxia and its harmful effects in many marine habitats (4).

Albeit overlooked for many years, ocean deoxygenation is now also recognized as a substantial threat to coral reefs (5,6), but how corals are able to regulate their internal O₂ levels in response to changes in external O₂ remains poorly understood (7). A key limitation is our ability to link the O₂ concentration in the surrounding water to the tissue-level O₂ concentration, which is affected by coral morphology and metabolism but also O₂ transfer across the tissue-water and tissue-skeleton interface.

Colonies of tropical reef-building corals are composed of hundreds to thousands of simple, calcifying polyp animals that harbor photosynthetic microalgae in their tissues, and the photosynthates translocated from the microalgal symbionts to the surrounding host cells are the major source of organic carbon for the animal. The polyps have tentacles with stinging cells that can catch prey, which is taken up via the mouth and digested in the gastric cavity releasing essential nutrients, which can be shared between different polyps in a coral colony via channels in their connective tissue (FIG. 1). Corals can thus exhibit strong tissue plasticity via expansion and contraction, which affects the surface area to volume ratio and thus the gas exchange between coral tissue and the surrounding seawater (8).

Point measurements with electrochemical and fiber-optic microsensors (9,10) showed that the O₂ status of corals undergoes strong dynamics during day-night cycles, where supersaturating O₂ levels build up during daytime due to the photosynthesis by their microalgal symbionts, while hypoxic (or even anoxic) conditions are observed during night-time due to respiration and limited O₂ transfer from the surrounding seawater. However, such point measurements in tissue can be invasive and are not representative of the complex 3D morphology and compartmentalization of corals (11), which also includes intricate cilia-driven external and internal flow patterns at the tissue surface and in the gastric cavity of corals (12,13). Chemical imaging with optical sensor particles (e.g. 14,15) offer an interesting alternative to such measurements.

While O₂-sensitive sensor particles have previously been applied for mapping the O₂ concentration and dynamics over the external tissue surface of corals (11,16,17) and aquatic plants (18), the mapping of internal O₂ concentration in living coral tissue and gastric cavities has so far not been realized. External application of sensor particles has the following complications in corals: (i) the response to changes in O₂ can be rather slow particularly for larger particles >5- 10 µm); (ii) mucus production can bind and slowly remove the particles from the coral surface and may also influence

the measurements; (iii) O₂ mapping inside the tissues is not possible as the mucus and epidermal tissue acts as a barrier.

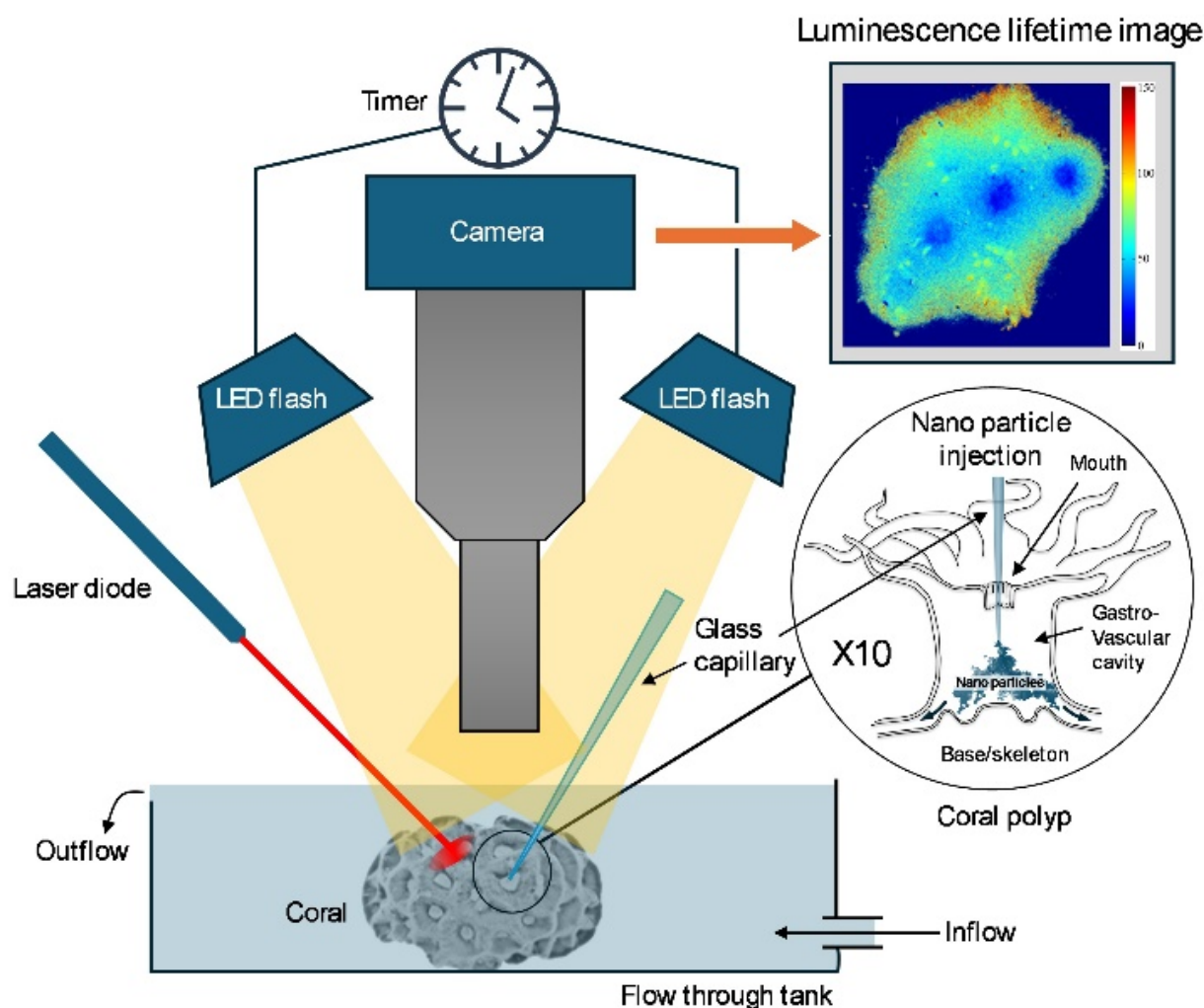


Figure 1. Schematic drawing of the setup used for injecting O₂ sensor nanoparticles into the gastrovascular cavity of coral polyps and subsequent mapping of the internal O₂ concentration with a luminescence lifetime system. The inset shows a coral polyp, where a glass microcapillary is introduced through the coral mouth into the gastrovascular cavity for injection of sensor nanoparticles, that can then distribute to neighboring polyps via channels in the connective tissue (see also SVIDEO 1). A laser pointer was used to locally stimulate photosynthetic O₂ production.

Oxygen nanosensors represent analytical tools, which can help to overcome the above limitations (19,20). Sensor nanoparticles can be injected directly into the tissue, and due to their small size the sensor particles respond virtually instantaneous to changing O₂ concentration. However, because of strong light scattering and absorption in tissues, luminescent sensors relying on UV-blue excitation and emission in the visible spectral range are poorly suitable for mapping O₂ inside tissues. As an alternative, optical indicators emitting in the NIR are promising materials for imaging O₂ in tissues (21). Such sensor materials are often based on dendrimers containing a phosphorescent benzoporphyrin complex as a core (22,23,24). Alternatively, polymeric nanoparticles can be doped

with a lipophilic O₂ indicator (25). Similarly to the shell of a dendrimer, the polymeric material protects the indicator from undesired interferences (e.g. quenchers, ionic species etc.) and controls O₂ permeability. This approach was preferred in the current work because of high flexibility in tuning the sensitivity of the probe and its spectral properties and the simplicity of the preparation methods (26). Furthermore, the indicator material is commercially available from several providers. Here we describe optical O₂ sensor particles that are suitable for internal, subsurface O₂ measurements in coral tissue and show their application in combination with luminescence lifetime imaging for studying the spatiotemporal dynamics of O₂ concentration within the tissues of two reef-building coral species.

EXPERIMENTAL SECTION

Reagents and chemicals

Luminescent oxygen indicator platinum(II)-tetra(4-fluoro)phenyltetrabenzoporphyrin (PtTPT-BPF) was prepared according to the previously published procedure (27). Poly(methyl methacrylate-co-methacrylic acid) (PMMA-MA; 10% methacrylic acid, MW ~100,000) was from Polysciences, Warrington, USA. The organic solvents were from Roth (Germany).

Preparation of nanoparticles

Oxygen-sensitive nanoparticles were prepared according to a previously published procedure (26). Briefly, 3 mg of PtTPTBPF and 200 mg of PMMA-MA were dissolved in 40 mL of tetrahydrofuran and the solution was diluted to 100 mL with acetone. Then, 700 mL of water was added within 2-3 s under vigorous stirring. The organic solvents and most water were removed under reduced pressure. The aqueous dispersion was concentrated to contain about 20 mg mL⁻¹ of particles.

The size and surface charge (Zeta-potential) of the sensor particles were measured via dynamic light scattering (DLS) on a particle size analyzer (Zetasizer Nano ZS; Malvern, UK).

Imaging setup

The imaging of O₂ concentration was done with a modular luminescence lifetime imaging system (28,29), which encompasses a fast gate-able CCD camera (1280 x 1028 pixels; SensiCam-SensiMod, PCO/Excelitas, Kehlheim, Germany), 2 high power LED excitation light sources (617 nm; Roitner LaserTechnik GmbH, Vienna, Austria) to provide homogeneous excitation of the sample., and a custom built trigger unit to synchronize excitation light exposure and image acquisition over defined time intervals. The camera was equipped with a macro lens (1.4/17 CCTV, Xenoplan, Schneider-Kreuznach, Germany) equipped with distance rings (5 mm + 0.5 + 1 mm) for higher magnification. With the chosen objective, the achieved field of view was about 2.5 x 2 cm yielding a resolution of 20 µm per pixel. A 720 nm long-pass filter (R-720; Edmund Optics, Barrington, USA) in combination with a plastic filter ("bright red"; Lee Filters, UK) was mounted in front of the lens. Given sufficient luminescence signal, the imaging system can acquire O₂ images with a time resolution of ~0.5 s (28).

The rapid lifetime determination method was used to calculate the luminescence decay time, τ , by measuring luminescence intensities in two windows (1-41 µs and 26-66 µs after the excitation, respectively). The decay time, i.e., the luminescence lifetime was calculated as (28):

$$\tau = \frac{t_2 - t_1}{\ln(I_1 / I_2)}, \quad (1)$$

where t_1 and t_2 is the time corresponding to the start of the 1st and the 2nd window, respectively (1 and 26 μ s in our setup), and I_1 and I_2 are the luminescence intensities within the respective time windows.

Calibration of the O₂-sensitive nanoparticles

A dispersion of the nanoparticles was placed inside a custom-made aluminium flow-through chamber equipped with a glass window. The cell was sparged with gas mixtures and the dispersion was stirred using a magnetic stirring bar for faster gas exchange. The gas mixtures were prepared from nitrogen (99.999% purity, Linde Gas, Austria) and compressed air using a gas mixing devices (Red-y, Aesch, Switzerland & Gasmixer, Sensor-Sense, Netherlands). The temperature of the cell and the gas mixtures was kept constant at 26 °C.

Sample preparation and experimental setup

Symbiont bearing corals *Goniastrea* sp. and *Pocillopora damicornis* were sampled from the reef flat off Heron Island, Great Barrier Reef, Australia. After sampling, the corals were kept at Heron Island Research Station in an outdoor aquarium continuously flushed with aerated seawater from the reef flat. Prior to the experiments a coral specimen was transferred to a flow chamber flushed with aerated seawater (pH ~ 8.1) at 26 °C and at a flow rate of approximately 3 cm s⁻¹. The dispersion of the nanoparticles was injected through a glass capillary into the mouth opening of a single coral polyp under stagnant conditions (Fig. 1). The injection process was monitored under a dissection microscope (SM-6TZ-54S; Amscope, Irvine, USA) equipped with a CCD camera. To visualize the channel network connecting individual polyps in the coral colony, we also injected India ink using a similar procedure (see SVideo 1). The coral was left in the flow chamber for several hours prior to imaging experiments.

Stimulation of photosynthesis activation of the coral colony samples was performed by repeating excitation of the coral with the light from the red LEDs used for image acquisition. Under constant LED illumination, the incident photon irradiance reached 1100-1200 μ mol photons m⁻² s⁻¹, as measured with a mini scalar irradiance sensor (US-SQS/L; Walz GmbH, Effeltrich, Germany) connected to a light meter (ULM-500; Walz GmbH, Effeltrich, Germany). Under pulsed illumination via the camera system, the illumination time is roughly only 1/5 of the total time and the incident photon irradiance level was thus ~220-240 μ mol photons m⁻² s⁻¹. Local activation of symbiont photosynthesis in single coral polyps was performed with a red laser pointer (660 nm) for 1, 3, 6 and 10 min with a photon irradiance of 350 μ mol photons m⁻² s⁻¹.

Data processing

Image processing of the acquired images was done in Matlab 7.10 (Mathworks, USA) to obtain pseudocolor O₂ concentration images based on the measured luminescence lifetime images and the calibration.

RESULTS AND DISCUSSION

Oxygen-sensitive nanoparticles

To be suitable for sub-surface imaging of O₂ distribution in coral tissue, the O₂ nanosensors should fulfil the following requirements: (i) be dispersible in water; (ii) be small enough to be distributed within the coral after injection; (iii) possess excitation and emission in the red and NIR part of the spectrum to minimize the light loss in the tissue due to absorption and scattering; (iv) have good luminescence brightness enabling low to moderate excitation light levels to minimize actinic effects (e.g. stimulation of algal photosynthesis) during the measurements; and (v) possess a suitable

dynamic range rate ranging from anoxia to O₂ concentrations significantly exceeding air saturation, i.e., mimicking the O₂ dynamics experienced by corals in their tissue during day-night cycles (9). Based on the above requirements, we designed a new nanoparticle sensor material for O₂ measurements in coral tissues (Fig. 2). The nanoparticle sensors are composed of the O₂-sensitive dye, platinum(II) tetra(4-fluorophenyl)tetrabenzoporphyrin (PtTPTBPF)(27), incorporated into poly(methyl methacrylate-co-methacrylic acid) (PMMA-MA) nanoparticles via precipitation (26). The dye absorbs in the blue and in the red part of the spectrum and shows phosphorescence in the NIR region (Fig. 2a). These spectral properties make the sensor nanoparticles well suited for intra-tissue measurements. Moreover, the O₂ indicator possesses very good luminescence brightness (i.e., the product of molar absorption coefficient ϵ and the luminescence quantum yield QY). Indeed, $\epsilon = 146,000 \text{ M}^{-1}\text{cm}^{-1}$ for the Q band (615 nm) (26) and the QY is about 21% (30).

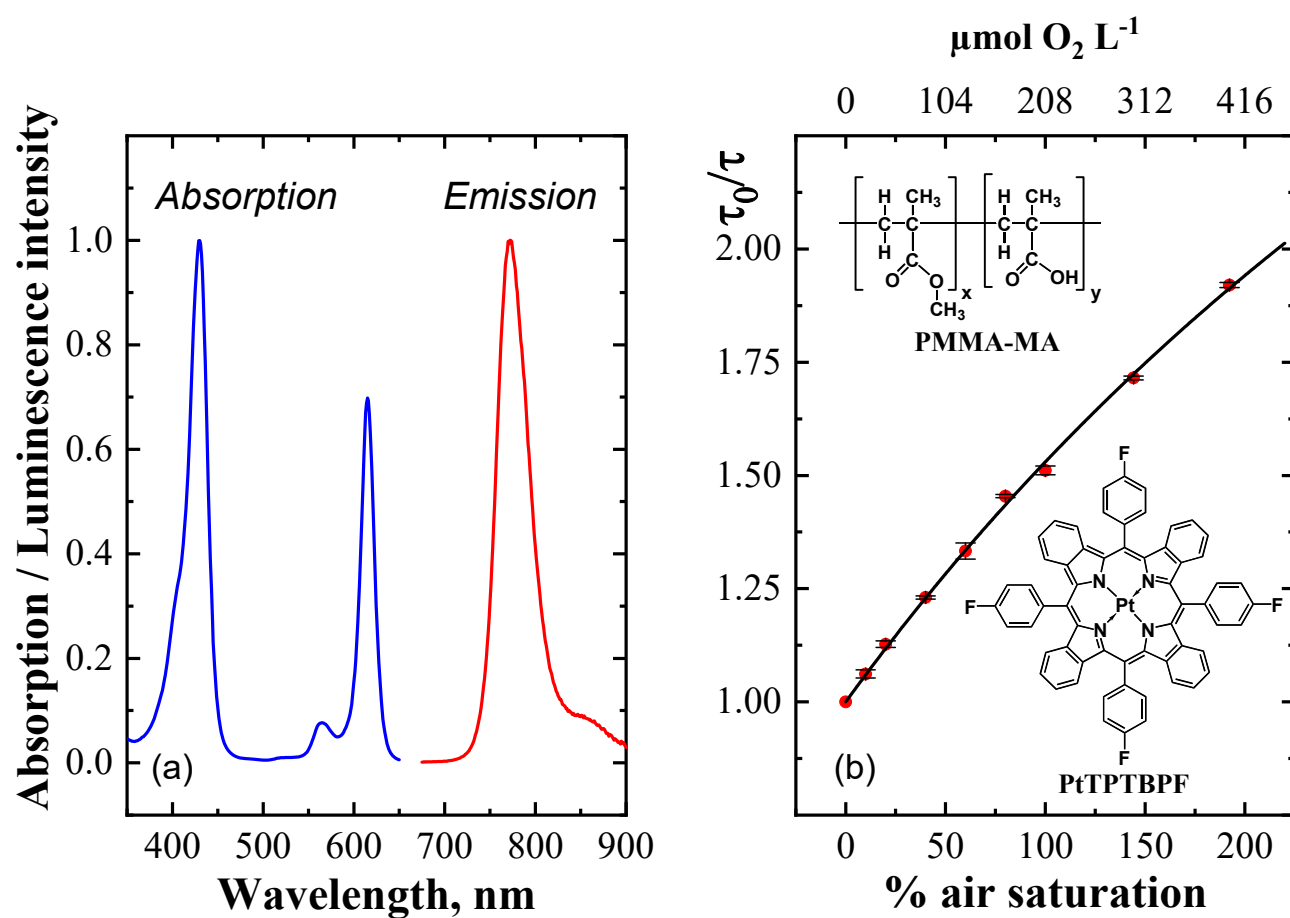


Figure 2. Spectral properties of the O₂-sensitive dye, platinum(II) tetra(4-fluorophenyl)tetrabenzoporphyrin (PtTPTBPF) in toluene (a) and a Stern-Volmer plot of the luminescence lifetime, τ , for the O₂-sensitive nanoparticles in seawater at 26 °C and a salinity of 35 as a function of O₂ concentration (b). The solid line in panel (b) represents a fit of Eq. 2 to the experimental values. The insets show the chemical structures of the O₂ dye and the nanoparticle polymer components.

The charged groups, which are present in the copolymer (methacrylic acid), enabled us to prepare nanoparticles that disperse well in water. This was achieved by using a simple precipitation method, where the O₂ sensitive dye and the polymer are first dissolved in an organic solvent (tetrahydrofuran/acetone mixture) and are then precipitated by fast addition of water, with subsequent removal of the solvents and partly water under reduced pressure. The resulting nanoparticles are rather small (Z_{AV} ~65 nm, as determined by DLS measurements; SFig. 1) and negatively charged (Zeta potential of – 25 mV). Preliminary experiments with other nanoparticles, i.e., cationic RI-100 beads (31) showed that they are unsuitable for measurements in seawater due to strong aggregation in presence of high salt concentration.

The sensitivity of the O₂-sensing material is mostly determined by i) the luminescence decay time of the indicator (τ_0 about 54 μ s in the absence of O₂ for PtTPTBPF), and ii) the O₂ permeability of the polymer matrix. In our sensor nanoparticles, the O₂ permeability of PMMA-MA is lower than e.g. in commonly used polystyrene-based sensor nanoparticles or planar optodes (15). Consequently, the sensor particles exhibit a sufficiently strong change in luminescence at O₂ concentration exceeding air saturation. A Stern-Volmer plot of the quenching properties of the sensor particles (Fig. 2b) shows that they are suitable for measurements at 0 to >200% air saturation. The non-linear Stern-Volmer response was well described by the “two-site model” (32) assuming localization of the indicator in two significantly different environments. Assuming the negligible quenchability of the indicator in the second site and extending the fit to the luminescence decay time (albeit without any physical meaning) the following equation can be used:

$$\frac{I}{I_0} = \frac{\tau}{\tau_0} = \frac{f}{1 + K_{SV}[O_2]} + 1 - f, \quad (2)$$

where f and K_{SV} are the fraction of the total emission and the Stern-Volmer constant for the first site, respectively. Fitting Eq. 2 to our calibration data showed an excellent fit ($r^2 = 0.999$) yielding values of $f = 0.80$ and $K_{SV} = 0.0075$ % air saturation⁻¹.

Nanoparticle injection and distribution

A solution of nanoparticles dispersed in seawater was injected through a glass capillary directly into the mouth and gastric cavity of the coral, where they distributed inside the coral gastrovascular canal system connecting neighbouring polyps (Fig. 1). In this study we aimed to fill the gastrovascular cavity with sensor materials by continuing the injection until we could see particles coming out of the neighbouring polyps (SVideo 1). In the coral *Pocillopora damicornis*, the intensity in the injection point remained high for several hours (SFig. 2), whereas with the larger polyps of *Goniastrea* sp. a more homogeneous particle distribution was achieved within several minutes after the injection (Fig. 3). This probably reflects differences in the connectivity between individual polyps as well as different skeletal architecture and internal dimensions of the gastric cavities in the different coral species (33,34). Mucus produced during the injection were removed by the water flow, but the injected particles were retained within the coral tissue even after 24h, while no particles were evident on the external tissue surface of the corals. This is in contrast to magnetic microparticles used in previous work to map the O₂ conditions on the external coral tissue surface (16), which were partially trapped and slowly carried away with mucous when water flow was applied.

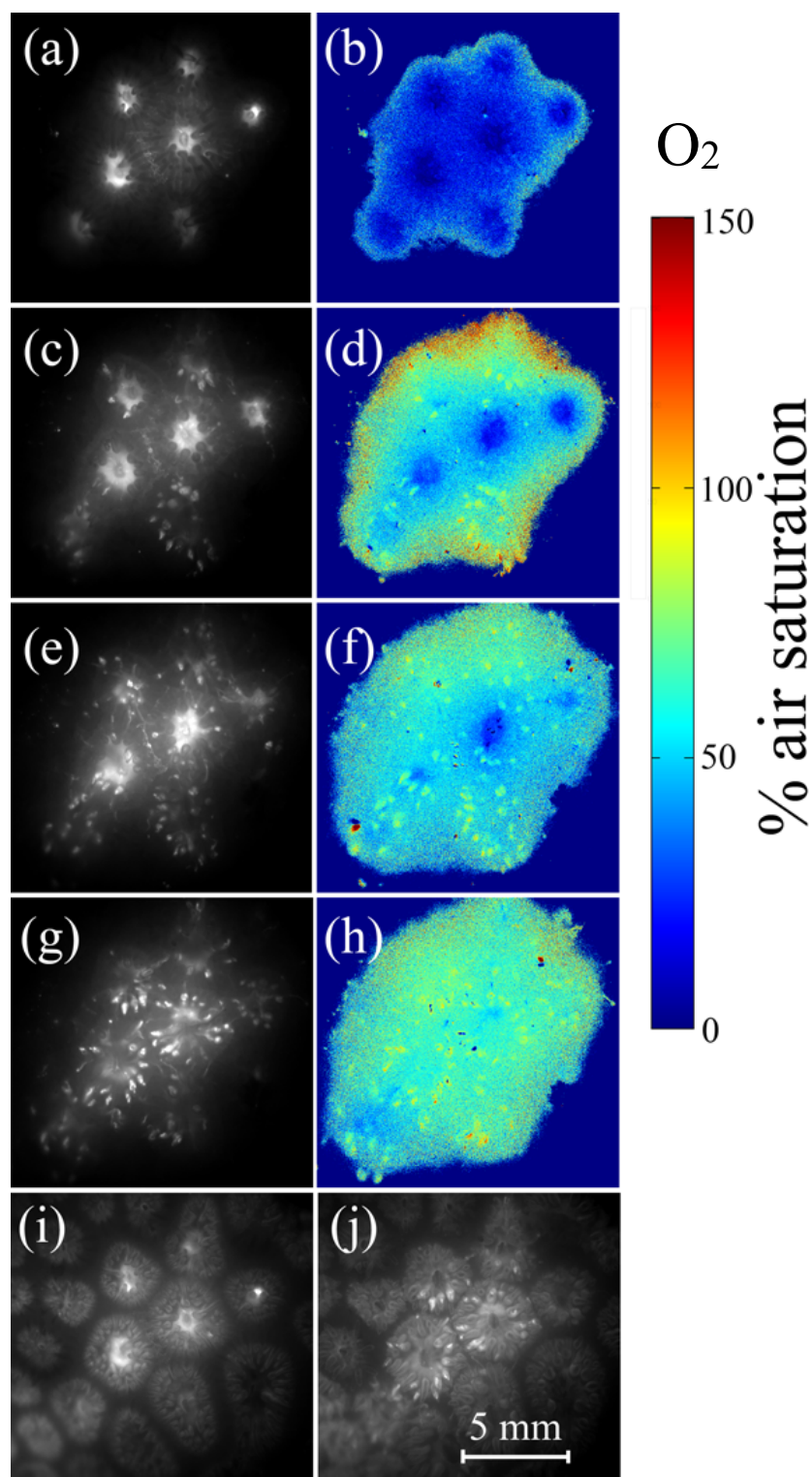


Figure 3. NIR (780 nm) luminescence intensity and subsurface O₂ dynamics in the coral *Goniastrea* sp. as a function of time after the injection of sensor particles. (a), (c), (e) and (g) show luminescence intensity images (recorded with 1 μ s delay after LED flash) at 10, 90, 180 and 280 min after the injection of sensor nanoparticles. (b), (d), (f) and (h) show corresponding pseudocolor images of the O₂ concentration. (i) and (j) show intensity images recorded during the excitation pulse at 10 and 280 min after the injection of sensor particles, respectively, revealing the coral structure.

Oxygen dynamics in corals after nanoparticle injection

Figure 3 shows NIR (780 nm) luminescence intensity images and the corresponding subsurface O₂ distribution in the coral *Goniastrea* sp., as derived from luminescence lifetime imaging, recorded immediately after the injection of sensor particles and during longer periods in darkness. Initially the coral polyps contracted and the coral tissue was hypoxic (about 5% and 20% air saturation for the coral mouth tissue and tentacles, respectively). Over the course of 2-3 hours in darkness, the coral tissue expanded as the mouth opened and tentacles stretched out into the overlying seawater. While initially highly concentrated in the mouth tissue, the sensor nanoparticles also became more dispersed within the coral tissue during this time, presumably by a combination of diffusion and active transport in the gastrovascular channels via cilia-induced advective transport (13,35).

The small size of the sensor nanoparticles also enables their dispersion from the gastric cavity into the coral tissue. In *Pocillopora damicornis*, we found that the O₂ concentration in the upper tissue layer was different than when focusing into deeper tissue layers (Fig. S1). This indicates the presence of an O₂ gradient, which was measured with sensor nanoparticles distributed within the tissue and in the gastrovascular system. However, our macroscopic imaging system was not optimized for precise z-stacking, and a more precise 3D quantification of the O₂ distribution in corals would require more sophisticated imaging systems such as confocal or light sheet microscopes (36). Furthermore, such high resolution measurements would also enable a more precise mapping of the nanoparticle distribution in the sample.

In *Goniastrea* sp., the sensor nanoparticles showed a tendency to accumulate in the tentacles (Fig. 3g,j), and the O₂ concentration increased to ~60 and 100% air saturation in the coral mouth tissue and tentacles, respectively, in darkness. The higher availability of O₂ within tentacles can be explained by their higher surface area to volume ratio securing a more efficient O₂ supply from the surrounding seawater (8).

The observed uneven distribution of luminescence intensity could be due to a heterogeneous distribution of nanoparticles or may be due to the orientation of the tentacles in direction of the camera lens with scattering effect within the tentacles so that the emission light is mostly outcoupled directly from the tentacle tips. While such heterogeneity, in combination with a strong autofluorescence of coral host pigments and chlorophyll in the microalgal symbionts, would severely complicate ratiometric imaging of O₂, the time-domain luminescence lifetime imaging approach enabled us to map the O₂ distribution without such interferences.

Light-dark O₂ dynamics in Goniastrea sp. coral

We stimulated the photosynthetic O₂ production of the symbiotic microalgae in the coral *Goniastrea* sp. with red light from the high power LED used for lifetime imaging. Figure 4 and 5 show the resulting O₂ dynamics during the light activation phase and subsequent relaxation in darkness. We found a fast response in the subsurface O₂ concentration in the coral tissue within a few seconds after onset of light or dark conditions. Even faster O₂ dynamics within a few seconds after a change in light conditions has previously been measured via point measurements with O₂ micro-sensors (9).

A more detailed analysis of the O₂ dynamics in specific regions of interest (ROI) 1 and 2 (outlined in Fig. 4b) showed initially higher oxygenation in the tentacles compared to the coral mouth, followed by a decrease of the oxygenation to similar values (about 130% air saturation) during the activation. Interestingly, analysis of the light-dark shifts shows that the O₂ content rapidly dropped to about 35% air saturation and then gradually increased again to 50-80% air saturation.

In the second experiment we doubled the photon flux ($220\text{--}240\text{ }\mu\text{mol photons}\cdot\text{m}^{-2}\cdot\text{s}^{-1}$) and observed a further increase in the oxygenation up to 200% air saturation (Fig. 5b). Again, a minimum O_2 concentration was reached after 300s in darkness, after which the O_2 concentration increased to about 65% air saturation. This dynamic can indicate significantly higher metabolic activity of the corals directly after the activation, e.g. via enhanced light and post-illumination respiration (37). Alternatively, the initial drop in O_2 concentration could also reflect a rapid local consumption, where the O_2 concentration drop gradually becomes alleviated by circulating water in the gastro vascular canals in the coral colony (13).

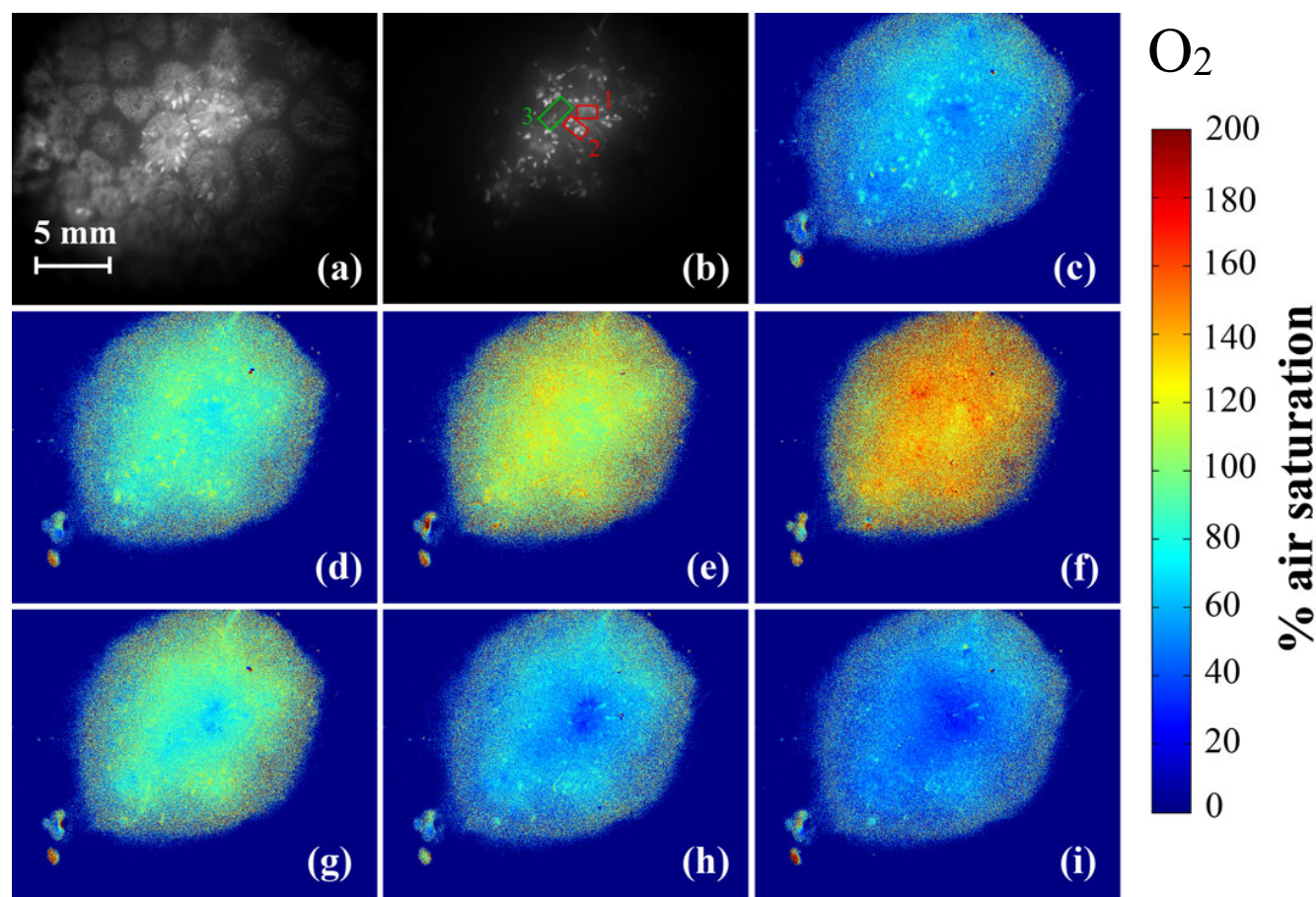


Figure 4. Subsurface O_2 dynamics during light-dark shifts in the coral *Goniastrea* sp. (a), structure of the coral revealed by an intensity image; (b), phosphorescence intensity image ($1\text{ }\mu\text{s}$ delay) and the 3 regions of interest; (c) –(i), pseudocolor images of the O_2 distribution during light activation with a photon irradiance (617 nm) of $110\text{--}120\text{ }\mu\text{mol photons}\cdot\text{m}^{-2}\cdot\text{s}^{-1}$ after 0, 65, 135, and 260 s for (c), (d), (e) and (f), respectively, and during the subsequent dark phase after 50, 70, and 130 s for (g), (h) and (i), respectively.

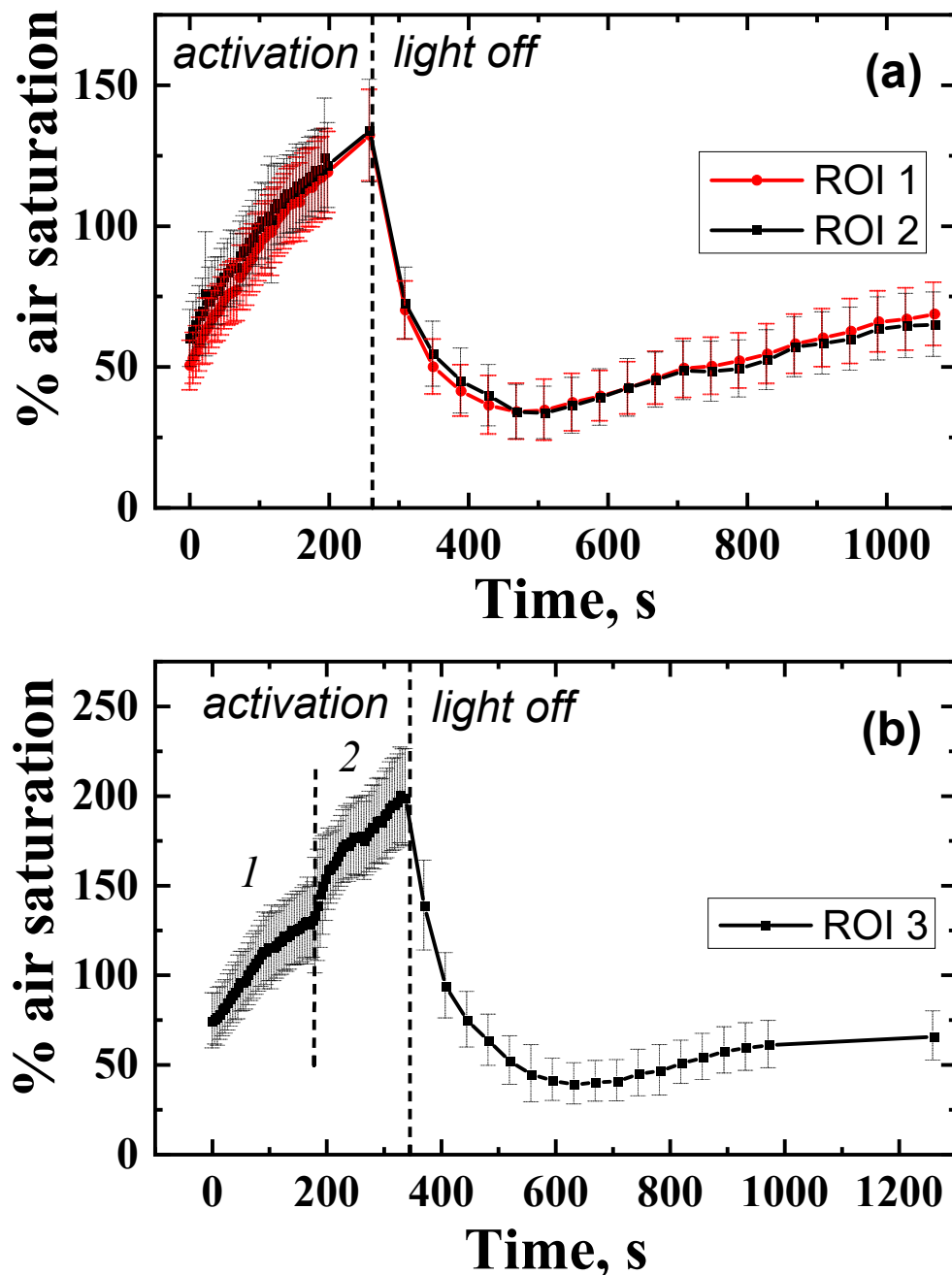


Figure 5. Subsurface O₂ dynamics in specific tissue ROI's (outlined in Fig. 4b) of the coral *Goniastrea* sp. light-dark shifts. In panel (a) the photon irradiance during activation was 110-120 $\mu\text{mol photons}\cdot\text{m}^{-2}\cdot\text{s}^{-1}$, while in panel (b) the respective values were 110-120 $\mu\text{mol photons}\cdot\text{m}^{-2}\cdot\text{s}^{-1}$ (period 1) and 220-240 $\mu\text{mol photons}\cdot\text{m}^{-2}\cdot\text{s}^{-1}$ (period 2). Symbols with error bars indicate means \pm standard deviation within the ROI.

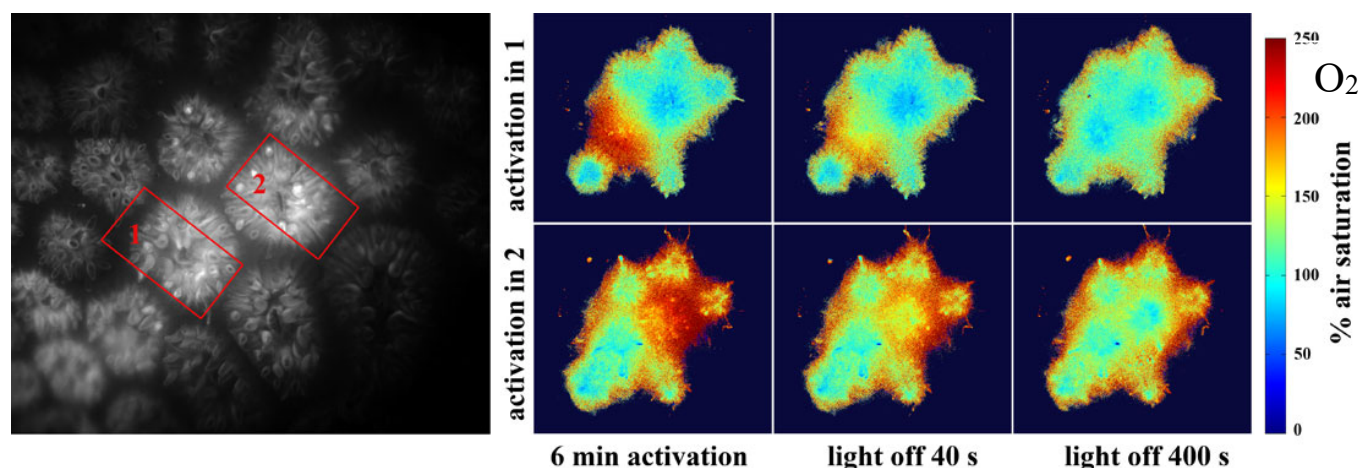


Figure 6. Luminescence intensity image showing internal tissue structure of the coral *Goniastrea* sp. indicating 2 ROI's where photosynthesis was activated (left). Pseudocolor images of the O₂ distribution in the two ROIs immediately after activation and during a subsequent dark phase. A red laser pointer (λ_{max} 660 nm) was used for local activation of photosynthesis with a photon irradiance of $350 \mu\text{mol photons m}^{-2} \text{s}^{-1}$, while the rest of the coral sample was in darkness.

We also performed local activation of photosynthesis in individual coral polyps in *Goniastrea* sp. colonies using a red (660 nm) laser pointer with a defined photon irradiance ($350 \mu\text{mol photons} \cdot \text{m}^{-2} \cdot \text{s}^{-1}$). The corresponding oxygenation values revealed that 1 min of continuous activation was not sufficient to saturate photosynthesis (Fig. 6, 7), while internal tissue O₂ levels obtained after 3, 6 and 10 min of local illumination were virtually identical (190-220 % air saturation) indication the onset of a steady state between local production, consumption and transport of O₂. The consumption of O₂ via respiration after onset of darkness was similar in different polyps (Fig. 7).

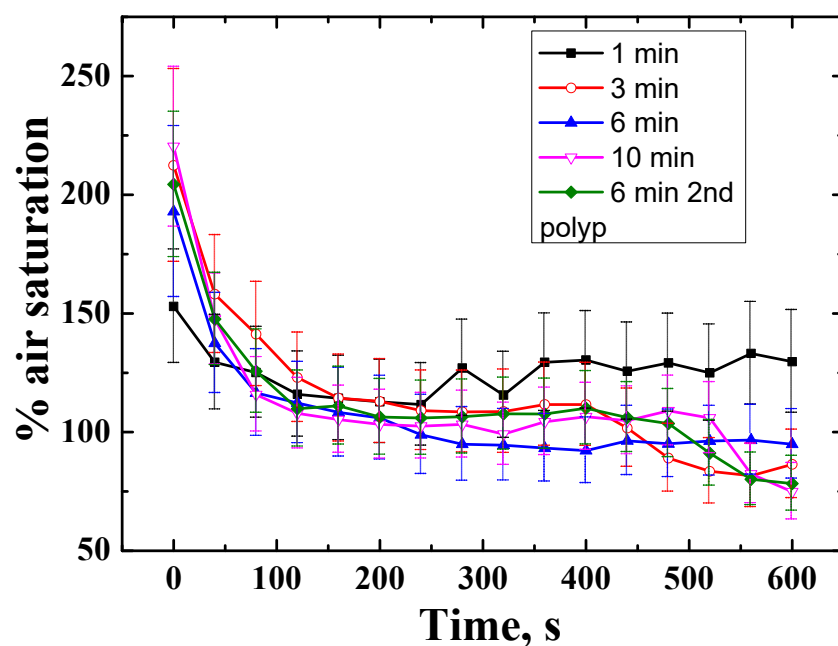


Figure 7. Oxygen dynamics during the light-dark shifts for 2 different polyps (see Fig. 6) at varying duration of the activation with a red laser pointer (660 nm; $350 \mu\text{mol photons m}^{-2} \text{s}^{-1}$). Symbols with error bars indicate means \pm standard deviation within the ROI.

CONCLUSION AND OUTLOOK

We showed that O₂-sensitive nanoparticles based on a NIR luminescent indicator represent promising tools for macroscopic *in vivo* imaging of the internal O₂ dynamics in corals. The sensor nanoparticles can be injected via the coral mouth and are distributed within the coral tissue via a network of gastro vascular canals connecting individual polyps in the coral colony. Lifetime imaging enables non-invasive mapping of the internal O₂ distribution in different parts of the corals without interference from background fluorescence, and the red excitation and NIR emission of the sensor nanoparticles ensured good tissue penetration. A similar approach using other types of sensor nanoparticles suitable for aquatic systems (15) can be used for mapping other relevant parameters such as the internal pH or temperature distribution in corals, which are additional key factors affecting coral health. Such measurements are key to improve our understanding of how coral tissue structure and plasticity regulate the internal chemical microenvironment and metabolic activity of corals and their endosymbionts – and how they are affected by environmental stress such as ocean warming, acidification and deoxygenation.

In this proof-of-concept paper, we focused on 2D macroscopic imaging covering larger coral tissue areas. We are now working on extending such measurements with higher resolution 3D luminescence lifetime imaging on suitable microscope platforms. Such measurements will enable a more detailed description of the internal O₂ distribution relative to the water-filled gastric cavity and the tissue layers of the coral.

Our experimental approach can also be adapted for O₂ mapping in other natural systems such as biofilms, plant and animal tissues, as well as in organoids and other cell constructs, where imaging internal O₂ conditions are relevant but challenging due to high optical density and background fluorescence.

Supporting Information.

SVideo 1; supplementary video showing injection of particles into corals. SFig.1; supplementary figure showing images of O₂ dynamics and structure in the coral *Pocillopora damicornis*.

This material is available free of charge at <http://pubs.acs.org>.

AUTHOR INFORMATION

Corresponding Author

* Michael Kühl - Marine Biological Section, Department of Biology, University of Copenhagen, Strandpromenaden 5, DK-3000, Helsingør, Denmark.

E-mail: mkuhl@bio.ku.dk

Orcid ID: [0000-0002-1792-4790](https://orcid.org/0000-0002-1792-4790)

* Sergey M. Borisov - Institute of Analytical Chemistry and Food Chemistry, Graz University of Technology, Stremayrgasse 9, A-8010, Graz, Austria.

E-mail: sergey.borisov@tugraz.at

Orcid ID: [0000-0001-9318-8273](https://orcid.org/0000-0001-9318-8273)

Author Contributions

MK and SB designed research, SB, DN and MK conducted experiments, SB and MK analyzed data and wrote the manuscript with editorial input from DN. / All authors have given approval to the final version of the manuscript.

Funding Sources

Gordon and Betty Moore Foundation (MK; grant no. GBMF9206;

<https://doi.org/10.37807/GBMF9206>);

MSCA-DN Flimaging3D funded by the European Union's Horizon 2020 research and innovation programme (MK; grant agreement no.101073507);

Villum Foundation (MK; VIL57413);

Independent Research Fund Denmark (MK; DFF-8022-00301B)

Notes

The authors declare no competing financial interest.

ACKNOWLEDGMENT

We thank Birgit Ungerböck (Graz University of Technology) for help with image processing. The staff of Heron Island Research Station (University of Queensland) is thanked for their logistic support during the field and lab work. The research was conducted under research permits for field work on the Great Barrier Reef, Australia (G11/34670.1 and G09/31733.1).

ABBREVIATIONS

LED light emitting diode; PtTPTBPF platinum(II) tetra(4-fluorophenyl)tetrabenzoporphyrin; PMMA-MA poly(methyl methacrylate-co-methacrylic acid); ROI region of interest.

REFERENCES

1. Fenchel, T.; Finlay, B. Oxygen and the Spatial Structure of Microbial Communities. *Biol. Rev. Camb. Philos. Soc.* **2008**, *83*, 553–569. DOI: 10.1111/j.1469-185X.2008.00054.x
2. Jo, J.; Price-Whelan, A.; Dietrich, L. E. P. Gradients and Consequences of Heterogeneity in Biofilms, *Nat. Rev. Microbiol.* **2022**, *20*(10), 593–607. DOI: 10.1038/s41579-022-00692-2
3. Keeling, R. E., Körtzinger, A., Gruber, N. Ocean Deoxygenation in a Warming World. *Ann. Rev. Mar. Sci.* **2010**, *2*, 199–229. DOI: 10.1146/annurev.marine.010908.163855
4. Morée, A. L.; Clarke, T. M.; Cheung, W. W. L.; Frölicher, T. L. Impact of Deoxygenation and Warming on Global Marine Species in the 21st Century, *Biogeosci.*, **2023**, *20*, 2425–2454. DOI: 10.5194/bg-20-2425-2023
5. Hughes, D. J.; Alderdice, R.; Cooney, C.; Kühl, M.; Pernice, M.; Voolstra, C. R.; Suggett, D. J. Coral Reef Survival under Accelerating Ocean Deoxygenation. *Nat. Clim. Change*, **2020**, *10*, 296–307. DOI: 10.1038/s41558-020-0737-9
6. Pezner, A. K.; Courtney, T. A.; Barkley, H. C.; Chou, W.-C.; Chu, H.-C.; Clements, S. M.; Cyronak, T.; DeGrandpre, M. D.; Kekuewa, S. A. H.; Kline, D. I.; Liang, Y.-B.; Martz, T. R.; Mitarai, S.; Page, H. P.; Rintoul, M. S.; Smith, J. E.; Soong, K.; Takeshita, Y.; Tresguerres, M.; Wei, Y.; Yates, K. K.; Andersson, A. J. Increasing Hypoxia on Global Coral Reefs under Ocean Warming. *Nat. Clim. Change*, **2023**, *13*(4), 403–409. DOI: 10.1038/s41558-023-01619-2.
7. Hughes, D. J.; Cobbs, G.; Alexander, J.; Kühl, M.; Cooney, C.; Pernice, M.; Varkey, D.; Voolstra, C.; Suggett, D. Widespread Oxyregulation in Tropical Corals under Hypoxia. *Mar. Pollut. Bull.*, **2022**, *179*, 113722. DOI: 10.1016/j.marpolbul.2022.113722
8. Patterson, M. R. A Chemical Engineering View of Cnidarian Symbioses. *Am. Zool.*, **1995**, *32*(4), 566–582.h

9. Kühl, M.; Cohen, Y.; Dalsgaard, T.; Jørgensen, B. B.; Revsbech, N. P. The Microenvironment and Photosynthesis of Zooxanthellae in Scleractinian Corals Studied with Microsensors for O₂, pH and Light. *Mar. Ecol. Progr. Ser.*, **1995**, *117*, 159-172.
10. Kühl, M. Optical Microsensors for Analysis of Microbial Communities. *Meth. Enzymol.*, **2005**, *397*, 166-199.
DOI: 10.1016/S0076-6879(05)97010-9
11. Hughes, D. J.; Raina, J.-B.; Nielsen, D. A.; Suggett, D. J.; Kühl, M. Disentangling Compartment Function in Sessile Marine Invertebrates. *Trends Ecol. Evol.*, **2022**, *37*, 740-748.
DOI: 10.1016/j.tree.2022.04.008
12. Pacherres, C. O.; Ahmerkamp, S.; Koren, K.; Richter, C.; Holtappels, M. Ciliary Flows in Corals Ventilate Target Areas of High Photosynthetic Oxygen Production. *Curr. Biol.*, **2022**, *32*(19), 4150-4158. DOI: 10.1016/j.cub.2022.07.071
13. Boudier, T.; Petersen, J.; Faure, L.; Abed-Navandi, D.; Bouchnita, A.; Mueller, B.; Nazarov, M.; Englmaier, L.; Tesarova, M.; Frade, P. R.; Zikmund, T.; Koehne, T.; Kaiser, J.; Fried, K.; Wild, C.; Pantos, O.; Hellander, A.; Bythell, J.; Adameyko, I. Surface Flow for Colonial Integration in Reef-Building Corals. *Curr. Biol.*, **2022**, *32*(12), 2596-2609.e7.
DOI: 10.1016/j.cub.2022.04.054
14. Koren, K.; Kühl, M. Optical O₂ Sensing in Aquatic Systems and Organisms. In: D. B. Papkovsky and R. Dmitriev (ed.), Quenched-Phosphorescence Detection of Molecular Oxygen: Applications in Life Sciences. Royal Society of Chemistry, Detection Science Series, **2018**, *11*, 145-174.
15. Mosshammer, M.; Brodersen, K. E.; Kühl, M.; Koren, K. Nanoparticle-based Luminescence Imaging of Chemical Species and Temperature in Aquatic Systems: A Review. *Microchim. Acta*, **2019**, *186*, 126. DOI: 10.1007/s00604-018-3202-y
16. Fabricius-Dyg, J.; Mistlberger, G.; Staal, M.; Borisov, S.; Klimant, I.; Kühl, M. Imaging of Surface O₂ Dynamics in Corals with Magnetic Micro Optode Particles. *Mar. Biol.*, **2012**, *159*, 1621-1631.
DOI: 10.1007/s00227-012-1920-y
17. Koren, K.; Jakobsen, S. L.; Kühl, M. In-vivo Imaging of O₂ Dynamics on Coral Surfaces Spray-Painted with Sensor Nanoparticles. *Sens. Act. B*, **2016**, *237*, 1095-1101.
DOI: 10.1016/j.snb.2016.05.147
18. Brodersen, K. E.; Kühl, M.; Trampe, E.; Koren, K. Imaging O₂ Dynamics and Microenvironments in the Seagrass Leaf Phyllosphere with Magnetic Optical Sensor Nanoparticles. *Plant J.*, **2020**, *106*, 1504-1519. DOI: 10.1111/tpj.15017
19. Aylott, J. W. Optical Nanosensors - an Enabling Technology for Intracellular Measurements. *Analyst*, **2003**, *128*, 309-312.
DOI 10.1039/B302174M
20. Borisov, S. M.; Klimant, I. Optical Nanosensors - Smart Tools in Bioanalytics. *Analyst*, **2008a**, *133*, 1302-1307. DOI: 10.1039/B805432K
21. Lebedev, A. Y.; Cheprakov, A. V.; Sakadzic, S.; Boas, D. A.; Wilson, D. F.; Vinogradov, S. A. Dendritic Phosphorescent Probes for Oxygen Imaging in Biological Systems. *ACS Appl. Mater. Interfaces*, **2009**, *1*, 1292-1304. DOI: 10.1021/am9001698
22. Sakadzic, S.; Roussakis, E.; Yaseen, M. A.; Mandeville, E. T.; Srinivasan, V. J.; Arai, K.; Ruvinskaya, S.; Devor, A.; Lo, E. H.; Vinogradov, S. A.; Boas, D. A. Two-photon High-resolution Measurement of Partial Pressure of Oxygen in Cerebral Vasculature and Tissue. *Nat. Methods*, **2010**, *7*, 755-759. DOI: 10.1038/nmeth.1490

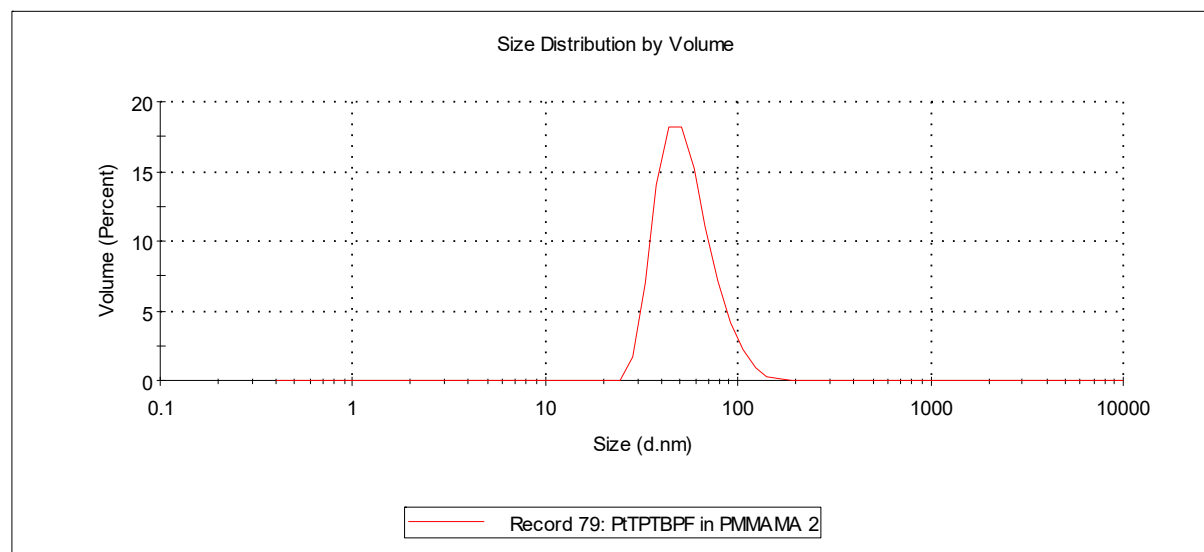
23. Esipova, T. V.; Karagodov, A.; Miller, J.; Wilson, D. F.; Busch, T. M.; Vinogradov, S. A. Two New 'Protected' Oxyphors for Biological Oximetry: Properties and Application in Tumor Imaging. *Anal. Chem.*, **2011**, *83*, 8756–8765. DOI: 10.1021/ac2022234
24. Lecoq, J.; Parpaleix, A.; Roussakis, E.; Ducros, M.; Houssen, Y. G.; Vinogradov, S. A.; Charpak, S. Simultaneous Two-Photon Imaging of Oxygen and Blood Flow in Deep Cerebral Vessels. *Nat. Med.*, **2011**, *17*, 893–898. DOI: 10.1038/nm.2394
25. Borisov, S. M.; Klimant, I. Luminescent Nanobeads for Optical Sensing and Imaging of Dissolved Oxygen. *Microchim. Acta*, **2008b**, *164*, 7–15. DOI: 10.1007/s00604-008-0047-9
26. Borisov, S. M.; Mayr, T.; Mistlberger, G.; Waich, K.; Koren, K.; Chojnacki, P.; Klimant, I. Precipitation as a Simple and Versatile Method for Preparation of Optical Nanochemosensors. *Talanta*, **2009a**, *79*, 1322–1330. DOI: 10.1016/j.talanta.2009.05.041
27. Borisov, S. M.; Nuss, G.; Haas, W.; Saf, R.; Schmuck, M.; Klimant, I. New NIR-emitting Complexes of Platinum(II) and Palladium(II) with Fluorinated Benzoporphyrins. *J. Photochem. Photobiol. A: Chem.*, **2009b**, *201*, 128–135. DOI: 10.1016/j.jphotochem.2008.10.003
28. Holst, G.; Kohls, O.; Klimant, I.; König, B.; Richter, T.; Köhl, M. A Modular Luminescence Lifetime Imaging System for Mapping Oxygen Distribution in Biological Samples. *Sens. Act. B*, **1998**, *51*, 163–170. DOI: 10.1016/S0925-4005(98)00232-9
29. Koren, K.; Mosshammer, M.; Scholz, V.; Borisov, S. M.; Holst, G.; Köhl, M. Luminescence Lifetime Based Chemical Imaging – a Comparison Between Time-domain and Frequency-domain Based Camera Systems. *Anal. Chem.*, **2019**, *91*, 3233–3238. DOI: 10.1021/acs.analchem.8b05869
30. Zach, P. W.; Freunberger, S. A.; Klimant, I.; Borisov, S. M. Electron-Deficient Near-Infrared Pt(II) and Pd(II) Benzoporphyrins with Dual Phosphorescence and Unusually Efficient Thermally Activated Delayed Fluorescence: First Demonstration of Simultaneous Oxygen and Temperature Sensing with a Single Emitter. *ACS Appl. Mater. Interfaces*, **2017**, *9*, 38008–38023. DOI: 10.1021/acsami.7b10669
31. Tsytsarev, V.; Arakawa, H.; Borisov, S.; Pumbo, E.; Erzurumlu, R.S.; Papkovsky, D.B. *In vivo* imaging of brain metabolism activity using a phosphorescent oxygen-sensitive probe. *J. Neurosci. Methods*, **2013**, *216*, 146–151.
32. Carraway, E.R.; Demas, J.N. Luminescence quenching mechanism for microheterogeneous systems. *Anal. Chem.*, **1991**, *63*, 332–336. DOI: 10.1021/ac00004a006
33. Yost, D. M.; Wang, L.-H.; Fan, T.-Y.; Chen, C.-S.; Lee, R. W.; Sogin, E.; Gates, R. D. Diversity in Skeletal Architecture Influences Biological Heterogeneity and *Symbiodinium* Habitat in Corals. *Zoology*, **2013**, *116*, 262–269. DOI: 10.1016/j.zool.2013.06.001
34. Dellaert, Z.; Putnam, H. M. Reconciling the Variability in the Biological Response of Marine Invertebrates to Climate Change. *J. Exp. Biol.*, **2023**, *226*, jeb245834. DOI: 10.1242/jeb.245834
35. Gladfelter, E. H. Circulation of Fluids in the Gastrovascular System of the Reef Coral *Acropora cervicornis*. *Biol. Bull.*, **1983**, *165*(3), 619–636. DOI: 10.2307/1541469
36. Dmitriev, R. I.; Intes, X.; Barroso, M. M. Luminescence Lifetime Imaging of Three-dimensional Biological Objects. *J. Cell Sci.*, **2021**, *134*(9), 1–17. DOI: 10.1242/jcs.254763
37. Schrameyer, V.; Wangpraseurt, D.; Hill, R.; Köhl, M.; Larkum, A. W. D.; Ralph, P. J. Light Respiratory Processes and Gross Photosynthesis in Two Scleractinian Corals. *PLoS One*, **2014**, *9*(10), e110814. DOI: 10.1371/journal.pone.0110814.

In-vivo Lifetime Imaging of the Internal O₂ Dynamics in Corals with NIR-emitting Sensor Nanoparticles

Michael Kühl^{*,a,b}, Daniel Aagren Nielsen^b and Sergey M. Borisov^{*,c}

^aMarine Biological Section, Department of Biology, University of Copenhagen, Strandpromenaden 5, 3000, Helsingør, Denmark. ^bClimate Change Cluster, University of Technology Sydney, Broadway, 2007, Australia. ^cInstitute of Analytical Chemistry and Food Chemistry, Graz University of Technology, Stremayrgasse 9, A-8010, Graz, Austria

SVideo 1. The video shows injection of India ink into a polyp of the coral *Pocillopora damicornis* via a thin glass capillary. The injected dye spreads to neighboring polyps via the gastrovascular network connecting individual polyps in the coral colony. The injection is continued until the ink appears out of the mouth of neighbouring polyps. Excess ink is rapidly flushed away by the flow of seawater over the coral sample.



SFigure 1. Size distribution for PMMA-MA nanoparticles doped with luminescent oxygen indicator platinum(II)-tetra(4-fluoro)phenyltetraabenzoporphyrin (PtTPTBPF), as determined by dynamic light scattering measurements.

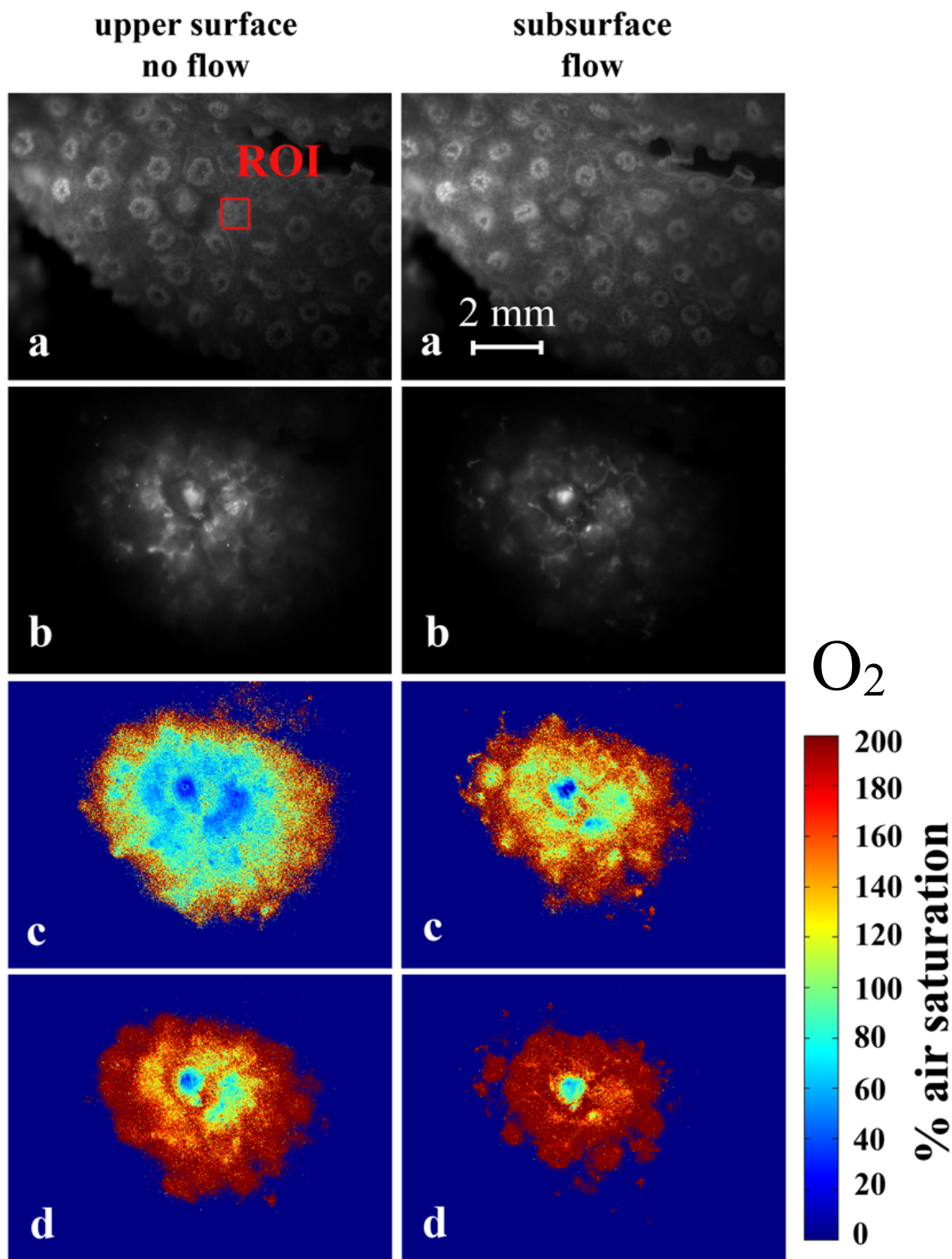


Figure 2. Structure and O₂ distribution in the tissue of the coral *Pocillopora damicornis* imaged with the camera focus in the upper (left) and lower (right) parts of the tissue. (a) structure as revealed by an intensity image (measured during red excitation); (b) phosphorescence intensity image (1 μ s delay); (c,d) pseudocolor images of the O₂ distribution before and after 170 s of light activation with a photon irradiance (617 nm) of 220-240 μ mol photons \cdot m⁻² \cdot s⁻¹.